Earth and Planetary Science Letters 331-332 (2012) 1–7

Contents lists available at SciVerse ScienceDirect

Earth and Planetary Science Letters

journal homepage: www.elsevier.com/locate/epsl

Spin states and hyperfine interactions of iron incorporated in $MgSiO_3$ post-perovskite

Yonggang G. Yu *, Han Hsu, Matteo Cococcioni, Renata M. Wentzcovitch

Department of Chemical Engineering and Materials Science, University of Minnesota, Minneapolis, MN 55455, USA

ARTICLE INFO

Article history:
Received 21 September 2011
Received in revised form 12 February 2012
Accepted 2 March 2012
Available online xxxx

Editor: L. Stixrude

Keywords:
Fe-bearing post-perovskite ($MgSiO_3$)
ferrous and ferric iron (Fe^{2+} and Fe^{3+})
spin state crossover
quadrupole splittings
equation of state
lower mantle
D″ layer
LDA + *U*

ABSTRACT

Using density functional theory + Hubbard *U* (DFT + *U*) calculations, we investigate the spin states and nuclear hyperfine interactions of iron incorporated in magnesium silicate ($MgSiO_3$) post-perovskite (Ppv), a major mineral phase in the Earth's D″ layer, where the pressure ranges from ~120 to 135 GPa. In this pressure range, ferrous iron (Fe^{2+}) substituting for magnesium at the dodecahedral (A) site remains in the high-spin (HS) state; intermediate-spin (IS) and low-spin (LS) states are highly unfavorable. As to ferric iron (Fe^{3+}), which substitutes magnesium at the A site and silicon at the octahedral (B) site to form $(Mg,Fe)(Si,Fe)O_3$ Ppv, we find the combination of HS Fe^{3+} at the A site and LS Fe^{3+} at the B site the most favorable. Neither A-site nor B-site Fe^{3+} undergoes a spin-state crossover in the D″ pressure range. The computed iron quadrupole splittings are consistent with those observed in Mössbauer spectra. The effects of Fe^{2+} and Fe^{3+} on the equation of state of Ppv are found nearly identical, expanding the unit cell volume while barely affecting the bulk modulus.

1. Introduction

Iron, the most abundant transition-metal element in the Earth, is widely present in major mantle minerals, including olivine, pyroxene, garnet, ferropericlase, magnesium silicate ($MgSiO_3$) perovskite (Pv), and the recently discovered $MgSiO_3$ post-perovskite (Ppv) with the $CaIrO_3$-type (Cmcm) structure (Murakami et al., 2004; Oganov and Ono, 2004; Tsuchiya et al., 2004). Owing to its incomplete 3*d* electron shell and comparable crystal field splitting energy and Hund's exchange energy, the total electron spin moment *S* of iron in minerals can vary with pressure and temperature. This phenomenon, known as spin-state crossover, has a great influence on physical and chemical properties of the host minerals. A well studied example is ferropericlase [(Mg,Fe)O], the second most abundant mineral in the lower mantle. In this mineral, ferrous iron (Fe^{2+}) undergoes a spin-state crossover from high-spin (HS), $S=2$, to low-spin (LS), $S=0$, at pressures near the mid mantle (45–55 GPa), which strongly affects the compressibility (Badro et al., 2003; Tsuchiya et al., 2006), elasticity, and sound velocity of this mineral (Crowhurst et al., 2008; Wentzcovitch et al., 2009; Wu et al., 2009). This HS–LS crossover also reduces the radiative thermal conductivity (Goncharov et al., 2006) and is expected to alter the partition of Fe and Mg between ferropericlase and $MgSiO_3$ Pv. In $MgSiO_3$ Pv, the dominant mineral phase in the lower mantle, recent studies have shown that the ferric iron (Fe^{3+}) substituting for silicon at the octahedral (B) site undergoes a spin-state crossover from HS ($S=5/2$) to LS ($S=1/2$) state at 50–60 GPa, while the Fe^{3+} substituting for magnesium at the dodecahedral (A) site remains HS (Catalli et al., 2010b; Hsu et al., 2011). This B-site spin-state crossover leads to an elastic anomaly in the Pv phase, which can be a possible source of seismic anomaly (Hsu et al., 2011). As to Fe^{2+} in Pv, which substitutes for magnesium at the A site, first-principles calculations have shown that no spin-state crossover occurs in the 0–150 GPa pressure range, namely, the A-site Fe^{2+} remains in the HS state (Hsu et al., 2010b). While a very large iron nuclear quadrupole splitting (QS) of 3.5–4.0 mm/s observed in Mössbauer spectra was suggested to be evidence for intermediate-spin (IS) Fe^{2+} (Lin et al., 2008; McCammon et al., 2008, 2010), first-principles calculations have shown this high-QS state to be HS Fe^{2+} (Bengtson et al., 2009; Hsu et al., 2010b).

The remaining piece of the puzzle for iron spin states in the deep mantle lies in the $MgSiO_3$ Ppv phase, possibly a main component of the Earth's D″ layer, which is a thermal boundary layer between the

* Corresponding author.
E-mail address: yuxxx135@umn.edu (Y.G. Yu).

0012-821X/$ – see front matter © 2012 Elsevier B.V. All rights reserved.
doi:10.1016/j.epsl.2012.03.002

mantle and the core and may be crucial for mantle dynamics (Lay and Garnero, 2007). Despite its importance, the iron spin states in Ppv are still unclear. Several possible spin states have been proposed in the past few years based on Mössbauer spectra, including IS Fe^{2+} (Lin et al., 2008; Mao et al., 2010), as well as HS Fe^{3+} at the A site and LS Fe^{3+} at the B site (Catalli et al., 2010a). In addition, metallic iron was also reported to occur in the compressed Ppv sample (Jackson et al., 2009). It should be noted that iron spin states cannot be identified merely based on measured QS values, as QS is not directly affected by the electron spin moment S, but directly proportional to the electric field gradient (EFG) at iron nucleus (see Section **2**). The EFG is determined by the electron density and orbital occupancy; its relation with iron spin may not necessarily be straightforward. Previous calculations of iron nuclear QS in Pv (Hsu et al., 2011) show that the IS and LS states of Fe^{3+} at the A site have very close QS values, ~2 mm/s, and both LS Fe^{2+} and HS Fe^{3+} possess low QS values, ~0.9 mm/s. Moreover, it has been shown that for $3d^6$ ions, such as Fe^{2+} in Pv (Hsu et al., 2010b) and Co^{3+} in $LaCoO_3$ (Hsu et al., 2010a), IS state does possess a lower EFG than HS state, which clearly indicates that associating high QS (~4 mm/s) with IS Fe^{2+} in Pv (Lin et al., 2008; McCammon et al., 2008) can be inaccurate. In this sense, first-principle calculations, combined with experimental data, is a necessary tool to identify iron spin states in complex minerals.

Several first-principle calculations based on density functional theory (DFT) (Kohn and Sham, 1965), have been conducted to study the iron spin states in $MgSiO_3$ Ppv (Caracas, 2010; Caracas and Cohen, 2008; Zhang and Oganov, 2006), with or without taking aluminum into consideration. In these calculations, however, the iron nuclear QS was not computed, and only standard DFT functionals, such as local density approximation (LDA) (Ceperley and Alder, 1980; Perdew and Zunger, 1981) and the Perdew–Burke–Ernzerhof (PBE) type GGA (Perdew et al., 1996), were adopted. It is well known that standard DFT functionals do not describe the on-site Coulomb interactions between 3d electrons properly, which can lead to difficulties in predicting correctly the electronic band gap as well as 3d orbital occupancy in iron-bearing minerals. The DFT + Hubbard U (DFT + U) method (Anisimov et al., 1991), on the other hand, provides more reliable predictions. An example is the HS Fe^{3+} at the B site in Pv, which was not found by GGA (Zhang and Oganov, 2006) but is identified in both experiment (Catalli et al., 2010b) and DFT + U calculations (Hsu et al., 2011). In addition, when the Hubbard U is determined self-consistently (U_{sc}) from the first-principles (Cococcioni and de Gironcoli, 2005), the predicted transition pressures satisfactorily agree with experiments for iron-bearing Pv (Hsu et al., 2010b, 2011). In this paper, we thus use the DFT + U_{sc} method to investigate iron spin states, hyperfine interactions, and relevant equation of states of iron-bearing $MgSiO_3$ Ppv.

2. Method

In our DFT + U calculations, both the LDA and the GGA functionals are adopted. The self-consistent U_{sc} parameter is determined by a linear response method (Campo and Cococcioni, 2010; Cococcioni and de Gironcoli, 2005; Hsu et al., 2011; Kulik et al., 2006), which is implemented in the QUANTUM ESPRESSO package (Giannozzi et al., 2009), a DFT code using the plane-wave pseudopotential method. Using the DFT + U_{sc} method, one can obtain electronically convergent HS, IS, and LS states for ferrous and ferric iron in a wide range of pressure/volume. For each spin state at each pressure, we perform damped variable cell shape molecular dynamics (Wentzcovitch et al., 1993) to make sure a minimum-enthalpy structure at the given spin state and pressure is achieved. At the end, we always compared the enthalpy of each identified spin state to determine the global minimum. The pseudopotentials used here are the same as those used in Umemoto et al., (2010). The energy cutoff is 40 Ry for the wave function and 160 Ry for the electron density. The **k**-point integration is performed on a shifted $4\times2\times2$ mesh (Monkhorst and Pack, 1976). The computed compression data are fitted to the third-order Birch–Murnaghan equation of state. All the spin states found via the plane-wave pseudopotential method are also independently confirmed via the augmented plane wave + local orbitals (APW + lo) method (Madsen et al., 2001) implemented in the WIEN2k code (Blaha et al., 2001), with which the electric field gradient (EFG), V_{zz}, at the center of iron nucleus is computed. The computed EFGs are converted to the QS value, ΔE_{QS}, using $\Delta E_{QS} \simeq eQV_{zz}/2$, where e and Q denote the electron charge and the nuclear electric quadrupole moment of iron, respectively. The widely accepted $Q = 0.16$ barn (Petrilli et al., 1998) and a slightly larger $Q = 0.18$ barn are adopted in this work (1 barn $\equiv 10^{-28}$ m^2).

3. Results and discussion

The $MgSiO_3$ Ppv has a layered structure, characterized by corner-sharing and edge-sharing SiO_6 octahedra extending on the ac plane (Fig. 1). Intercalated in between two adjacent SiO_6 layers are magnesium atoms at the dodecahedral (8–12 coordination) sites. Two substitution mechanisms have been studied in a 40-atom supercell: one Fe^{2+} substituting for one Mg^{2+} at the A site forming $(Mg_{0.875},Fe_{0.125})SiO_3$ [Fig. 1(a)] and two Fe^{3+} substituting for a pair of the nearest-neighbor Mg^{2+} (A-site) and Si^{4+} (B-site) forming $(Mg_{0.875},Fe_{0.125})(Si_{0.875},Fe_{0.125})O_3$ [Fig. 1(b)]. The calculated U_{sc} parameter is sensitive to spin and oxidation states as shown in Table 1, but barely depends on pressure (or volume). For each atomic configuration, we explored possible spin configurations of iron and determined the most favorable spin state. We then calculated the QS of each valence and spin state and compared them with those extracted from Mössbauer spectra. The 3d electron density distributions of iron in various spin states have been extracted to gain a qualitative understanding toward the connection between spin states and QS. Finally we inspected the effects of ferrous and ferric iron on the equation of state of Ppv. The inverse structure configuration of Fig. 1(a), in which Fe^{2+} occupies the B site and Si^{4+} occupies the A site, is highly unfavorable (~80 meV per atom higher in enthalpy than the normal structure) and is not considered here.

3.1. Spin states of Fe^{2+} in (Mg,Fe)SiO_3 Ppv

For Fe^{2+} in $(Mg_{0.875},Fe_{0.125})SiO_3$ Ppv shown in Fig. 1(a), four spin states were obtained: two HS states, one IS and one LS; their QS values were presented in Fig. 4a. The two HS states have distinct QSs: one has a QS of 3.09–3.67 mm/s, referred to as high-QS HS state, the other has a QS of 2.47–2.91 mm/s, referred to as low-QS HS state. Details on QS will be discussed later. Fig. 2 shows the relative enthalpies of these spin states with respect to the high-QS HS state. Several methods are used, including LDA + U and GGA + U with a trial $U = 4$ eV and $U = U_{sc}$. In the pressure range of this study (below 200 GPa), the high-QS HS state has the lowest enthalpy, whereas the relative enthalpies of the IS and LS states decrease under compression. The IS state is not attainable below 120 GPa by GGA + U [Fig. 2(b) and (d)], but it is attainable down to 0 GPa by LDA + U [Fig. 2(a) and (c)]. The enthalpy of the low-QS HS state is comparable with that of the high-QS HS state at low pressures, but increases with compression. Above ~160 GPa, the low-QS HS cannot be easily stabilized, for it converts to the high-QS HS state during structure optimization. Based on our enthalpy calculations, Fe^{2+} at the A site should always remain in the high-QS HS state below 200 GPa, and no spin moment reduction is expected, regardless of the choice of exchange correlation functional or Hubbard U.

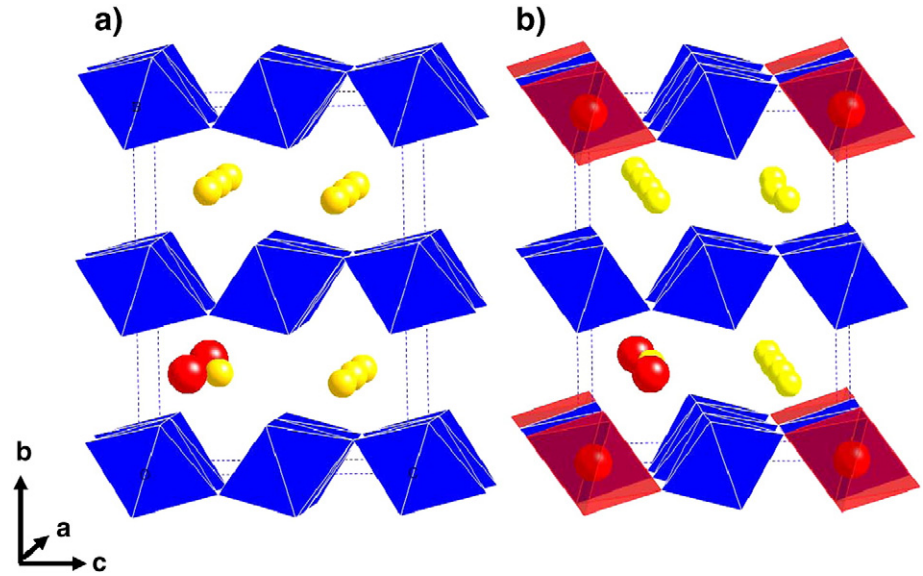

Fig. 1. Atomic configurations of iron-bearing Ppv. (a) $(Mg_{0.875},Fe_{0.125})\,SiO_3$ (40-atom cell), with Fe^{2+} at the A site; (b) $(Mg_{0.875},Fe_{0.125})(Si_{0.875},Fe_{0.125})O_3$, with two Fe^{3+} cations occupying A and B sites, respectively. Fe, Mg, and Si atoms are displayed in red, yellow, and blue spheres, respectively; blue and red octahedra represent respectively SiO_6 and FeO_6 units. (For interpretation of the references to color in this figure legend, the reader is referred to the web version of this article.)

3.2. Spin states of Fe^{3+} in (Mg,Fe)(Si,Fe)O_3 Ppv

The Ppv supercell (40-atom) with the presence of Fe^{3+} considered in this study is shown in Fig. 1(b), where two ferric iron substitute for the nearest-neighbor Mg^{2+} (A-site) and Si^{4+} (B-site) pair separated by 2.4 Å. Both parallel and anti-parallel alignments of the two Fe^{3+} cations have been considered. The anti-parallel state is only 1.8 meV (per formula unit) lower in enthalpy than the parallel state (at 150 GPa), indicating that the magnetic alignment barely affects the spin-state crossover, consistent with the previous study on the Pv phase [(Mg,Fe)(Si,Fe)O_3, (Hsu et al., 2011)]. The relative enthalpy of each spin state as shown in Fig. 3 corresponds to the anti-parallel configuration. It is difficult to stabilize HS Fe^{3+} at the B site. Starting with HS Fe^{3+} at both A and B sites, the B-site Fe^{3+} always drops to LS above 50 GPa. Further enthalpy calculations show that the B-site Fe^{3+} undergoes a HS to LS crossover at 36 GPa by GGA + U_{sc} and at −30 GPa by LDA + U_{sc}. Since Ppv is unquenchable experimentally at ambient conditions (Shim et al., 2008), this B-site spin-state crossover may not be observable in experiments. We have also investigated the spin configurations with IS or LS Fe^{3+} at the A site while the B-site Fe^{3+} remaining in LS, but both of them are energetically unfavorable. In addition, the configuration with IS at the A site and LS at the B site is unattainable below 150 GPa (Fig. 3). Therefore, we conclude that the A-site Fe^{3+} remains in the HS state, and the B-site Fe^{3+} remains in the LS state throughout the D″ pressure range.

3.3. Quadrupole splittings of iron

3.3.1. Comparison with data from Mössbauer spectra

As mentioned earlier, the spin state of a transition-metal ion cannot be directly determined by the quadrupole splitting or electric field gradient. First-principles calculations combined with experimental data, on the other hand, can provide useful guidance to unambiguously identify the spin state, as demonstrated in our previous works on iron and cobalt spin states (Hsu et al., 2010a, 2010b, 2011). The very same approach can be applied to study iron spin state in $MgSiO_3$ Ppv as well. The computed QSs of Fe^{2+} and Fe^{3+} in Ppv, along with the QSs extracted from Mössbauer spectra, are shown in Fig. 4. The Mössbauer spectra associated with samples free of Fe^{2+} clearly agree with the results shown in Fig. 3, that the A- and B-site Fe^{3+} are in HS and LS state, respectively, as the two observed QSs, 0.32–0.74 mm/s (Catalli et al., 2010a; Jackson et al., 2009) and 1.99 mm/s (Catalli et al., 2010a), are consistent with the computed QSs of A-site HS Fe^{3+}, 0.74–1.05 mm/s, and that of B-site LS Fe^{3+}, 1.92–2.28 mm/s (Fig. 4). This information regarding Fe^{3+} can be helpful to the analysis of more complicated samples where Fe^{3+} and Fe^{2+} coexist (Mao et al., 2010). In Mao et al. (2010), three distinct QSs, 3.77 ± 0.25, 2.53 ± 0.25, and 1.50 ± 0.25 mm/s are extracted from Mössbauer spectra. Based on the relative enthalpy and QS of each valence and spin state shown in Figs. 2–4, these three observed QSs should be attributed to the high-QS HS Fe^{2+} (at the A site), LS Fe^{3+} at the B site, and HS Fe^{3+} at the A site, respectively. Indeed, the observed QSs of Fe^{3+} in Mao et al. (2010) are higher than the computed ones. But based on our experience, the computed QSs can be easily increased by 0.2 mm/s if a larger Hubbard U is chosen (Hsu et al., 2010b). Besides, the QSs of Fe^{3+} observed in Mao et al. (2010) are also significantly higher than those observed in Catalli et al. (2010a) and Jackson et al. (2009) (see the caption of Fig. 4). In this sense, a combination of A-site HS Fe^{2+}, A-site HS Fe^{3+}, and B-site LS Fe^{3+} best explains the experimental and calculational results.

Table 1
The calculated self-consistent Hubbard U parameter (U_{sc}) for ferrous and ferric iron in Ppv at 120 GPa. The letters A and B represent A-site and B-site, respectively.

Fe^{2+}	A-HS	A-IS	A-LS		
U_{sc} (eV)	2.9	4.0	4.5		
Fe^{3+}	A-HS	A-IS	A-LS	B-HS	B-LS
U_{sc} (eV)	4.0	4.7	5.5	3.5	5.6

3.3.2. Iron nuclear QS and 3d electron density

As mentioned in Section **2**, iron nuclear QS is directly proportional to the EFG, $V_{zz} \equiv \partial^2 V/\partial z^2|_{\mathbf{r}=0}$, where V is the static potential resulting from electrons. For iron, V_{zz} is mainly contributed by 3d electrons, qualitatively based on

$$V_{zz} \propto \left(2n_{xy} + 2n_{x^2-y^2} - 2n_{3z^2-r^2} - n_{xz} - n_{yz}\right)/r^3, \quad (1)$$

where n_{xy}, n_{yz},... denote the orbital occupancy of d_{xy}, d_{yz},..., respectively. A detailed analysis of the 3d electron configuration in each

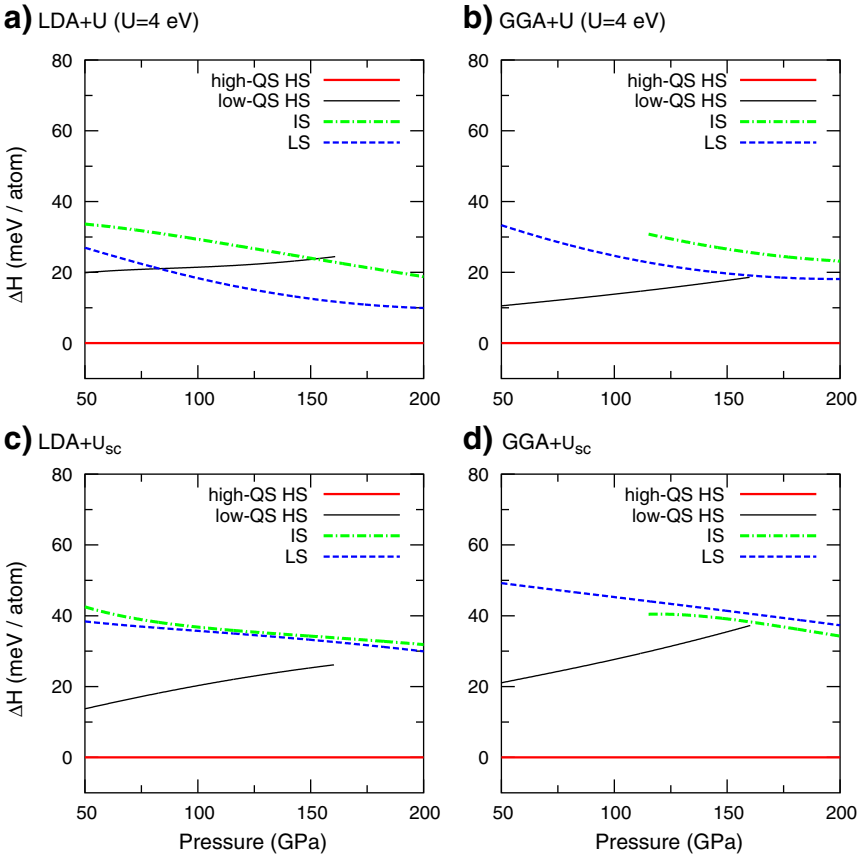

Fig. 2. Relative enthalpy of $(Mg_{0.875},Fe_{0.125})$ SiO_3 Ppv (40-atom cell) in each spin state. The high-QS HS state is used as a reference.

valence and spin state may thus help building an understanding toward the dependence of QS on spin states.

Fig. 5 illustrates the spin-up and spin-down 3d electron density isosurfaces of Fe^{2+} at A-site and Fe^{3+} at B-site in various spin states. In HS Fe^{2+}, the five spin-up electrons occupy five distinct 3*d* orbitals, forming a spherical shaped charge distribution [Fig. 5(a) and (b)], and barely contribute to the EFG. The QS of HS Fe^{2+} is thus mainly determined by the spin-down electron. In the high-QS HS state, the spin-down electron occupies the $d_{x^2-y^2}$ orbital [Fig. 5(a)], whereas the spin-down electron of the low-QS HS state occupies the $\sim\frac{1}{2}(d_{xz}+d_{yz})$ orbital, having a ring-shaped density distribution above and beneath the iron nucleus [Fig. 5(b)]. Evident from Eq. (1), the $d_{x^2-y^2}$ orbital contributes to the EFG twice as much as d_{xz} or d_{yz}, which explains the difference in QS for the two HS states.

The IS Fe^{2+} (at the A site) has four spin-up and two spin-down 3*d* electrons. The spin-up 3*d* electron density displays a spherical shaped distribution with holes that indicate the missing, spin-up d_{xy} orbital [Fig. 5(c)], whereas the spin-down electron density is dominated by the $d_{x^2-y^2}$ and $\sim\frac{1}{2}(d_{3z^2-r^2}+d_{yz})$ orbitals. Summing up the contributions to the EFG from these six 3*d* electrons based on Eq. (1), we

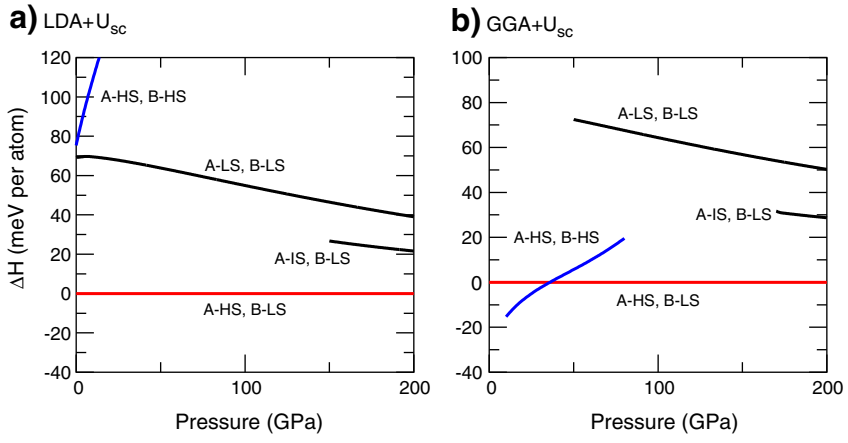

Fig. 3. Relative enthalpy of $(Mg_{0.875},Fe_{0.125})(Si_{0.875},Fe_{0.125})O_3$ Ppv (40-atom cell) in each spin state. The reference state has HS Fe^{3+} at the A site and LS Fe^{3+} at the B site.

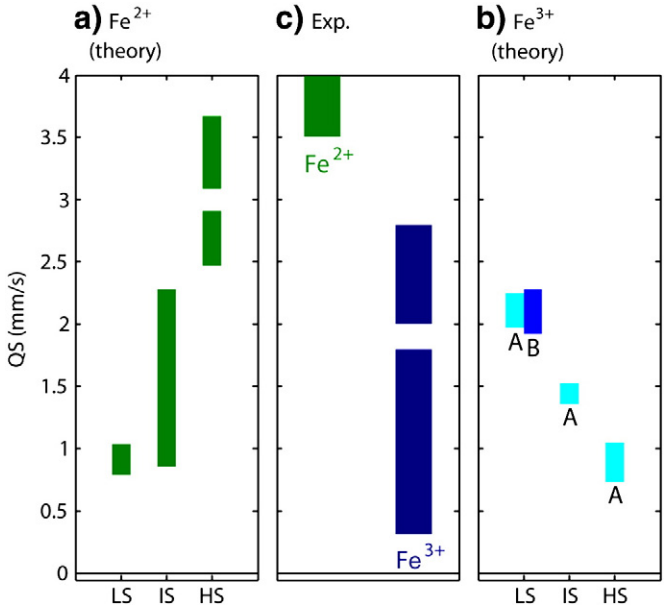

Fig. 4. The calculated QS values for Fe^{2+} (a) and Fe^{3+} (b) in Ppv in comparison with experiments (c). The letters A and B in (b) denote A-site and B-site for Fe^{3+}, respectively. The high-QS HS and the low-QS HS states produce two distinct QS values for HS Fe^{2+} in (a). The QS values determined from experiments include those for HS Fe^{2+} at A-site: 3.5–4.0 mm/s (Lin et al., 2008; Mao et al., 2010); HS Fe^{3+} at A-site: 0.318 mm/s (Catalli et al., 2010a), 0.72–0.75 mm/s (Jackson et al., 2009), and 1.55 ± 0.25 mm/s (Mao et al., 2010); LS Fe^{3+} at B-site: 1.99 mm/s (Catalli et al., 2010a) and 2.53 ± 0.25 mm/s (Mao et al., 2010).

find the EFG is mainly determined by the $\sim\frac{1}{2}(d_{3z^2-r^2}+d_{yz})$ orbital. Again according to Eq. (1), this orbital contributes less to the EFG than does $d_{x^2-y^2}$, hence the IS Fe^{2+} has a smaller QS than the high-QS HS Fe^{2+}, which is consistent with the computed QS values, 0.86–2.28 mm/s for IS Fe^{2+} versus 3.09–3.67 mm/s for the high-QS HS Fe^{2+}. The LS Fe^{2+} has a very small QS of 0.8–1.0 mm/s because the three t_{2g}-like orbitals are doubly occupied [Fig. 5(d)] and barely contribute to the EFG, based on Eq. (1).

Analyzing the QS of Fe^{3+} is straightforward. HS Fe^{3+} only has spin-up electrons occupying the five 3*d*-orbitals, forming a spherically shaped charge distribution, which leads to a small QS. As to the LS Fe^{3+}, the spin-up electrons occupy three t_{2g} orbitals and barely contribute to the EFG. Its spin-down electrons occupying the d_{xy}-like and d_{yz}-like orbitals contribute to the EFG [Fig. 5e]. This is why the computed QS for the LS Fe^{3+} is 1.92–2.28 mm/s, larger than that of the HS Fe^{3+}, 0.74–1.05 mm/s.

3.4. Equation of state of iron-bearing Ppv

Although the transition pressures between different spin states depend strongly on the value of Hubbard *U* parameter as shown in Figs. 2 and 3, the equations of state with $U=4$ eV or U_{sc} are very similar (for the LDA equation of state is already very good). Fig. 6 shows the calculated equation of states (compression curves from LDA + U_{sc}) of $MgSiO_3$ Ppv with 0%, 9%, and 25% Fe^{2+} at the A site (in dashed and solid lines) along with two sets of room-temperature X-ray diffraction data in solid symbols (Fig. 6): one collected from samples free of iron (Ono et al., 2006), the other with 9% Fe^{2+} (Shim et al., 2008). Noted that the equation of states associated with 9% iron is obtained by interpolating those associated with 0% and 25% iron assuming Vegard's law. The increase in volume of Ppv due to Fe^{2+} incorporation is estimated to be 0.054 vol.% for every 1% Fe^{2+}. Compared with experiments, the calculation underestimates the volume as the temperature effect has not been included. The calculated static bulk moduli (at 0 K) of Ppv with zero and 12.5% Fe^{2+} are 695 and 690 GPa at the pressure of 125 GPa, respectively, which is in agreement with the experimental value of 657 ± 16 GPa (Shim et al., 2008), considering that finite temperature can soften the bulk modulus by a few percent (Yu and Wentzcovitch, 2006). This result is also consistent with the recent first-principles calculation on elasticity of Fe-bearing olivine (Núñez-Valdez et al., 2010), which

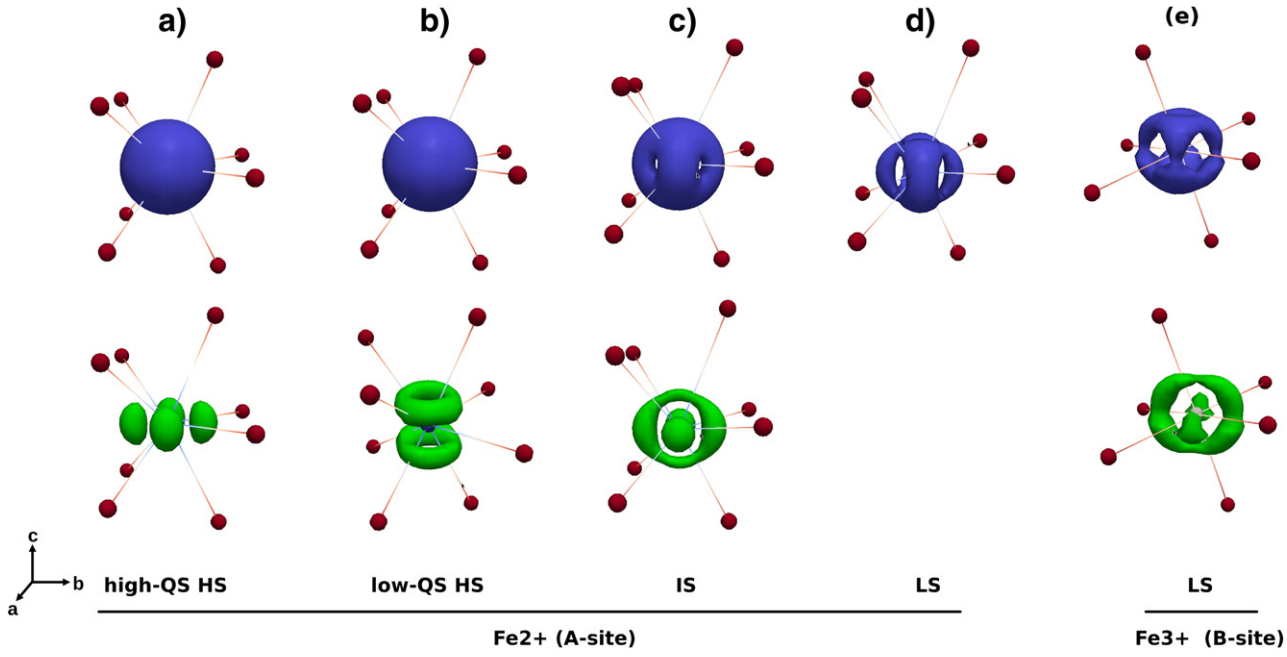

Fig. 5. Isosurface maps of the 3*d*-electron density of iron in Ppv: blue represents the spin-up electron density; green spin-down. Iron atoms are at the centers surrounded by oxygen atoms shown in red spheres. In (a) and (b), the spin-up orbitals show spherical shaped distribution, whereas the spin-down orbitals are $d_{x^2-y^2}$ and $\sim\frac{1}{2}(d_{xz}+d_{yz})$, respectively. In (c), the holes in the spin-up electron density result from the void of the d_{xy} orbital, and the two spin-down electrons occupy the $d_{x^2-y^2}$ and $\sim\frac{1}{2}(d_{3z^2-r^2}+d_{yz})$ orbitals. In (d) the spin-up and spin-down electron densities are degenerate, formed by three t_{2g}-like orbitals. In (e) the spin-up electron density is formed by three t_{2g}-like orbitals, and the spin-down by d_{xy}-like and d_{yz}-like orbitals. (For interpretation of the references to color in this figure legend, the reader is referred to the web version of this article.)

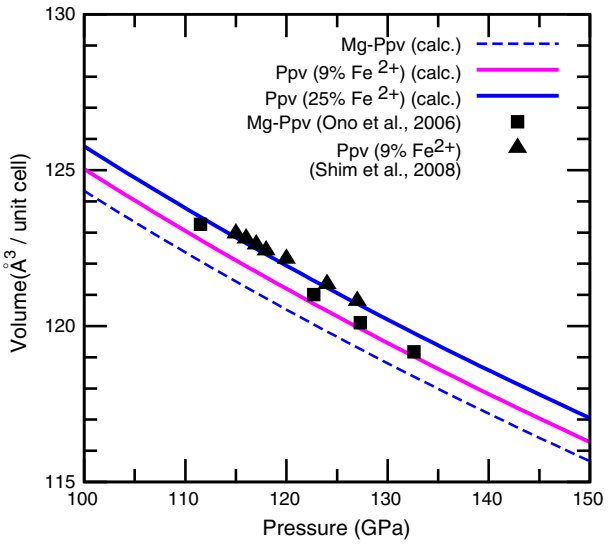

Fig. 6. The calculated volume-pressure relation (LDA + U_{sc}) for ferrous iron-bearing Ppv containing 0%, 9%, and 25% Fe^{2+} at the A site. The experimental data are shown in symbols: Ppv with 9% Fe^{2+} (Shim et al., 2008) and 0% iron (Ono et al., 2006).

shows 12.5% iron impurity reduces the shear modulus of olivine by 4–6% but barely affects the bulk modulus.

We also calculated the equation of state of Ppv containing 17% Fe^{3+} (Fig. 7), the same ferric iron concentration as in the experiment (Catalli et al., 2010a). Good agreement with experiment was obtained in both volume (see the two solid lines in Fig. 7) and bulk modulus, 691 GPa from the calculation versus 682 GPa from the experiment, both at the pressure of 125 GPa. The unit-cell volume of Ppv expands 0.047% for each percent of ferric iron incorporated in the structure, meaning Fe^{3+} is comparable to Fe^{2+} in expanding the volume of Ppv. It was previously proposed (Catalli et al., 2010a) that Fe^{3+} has little effect on volume of Ppv. The inconsistency between experiments and calculation may result from the different pressure scales in experiments.

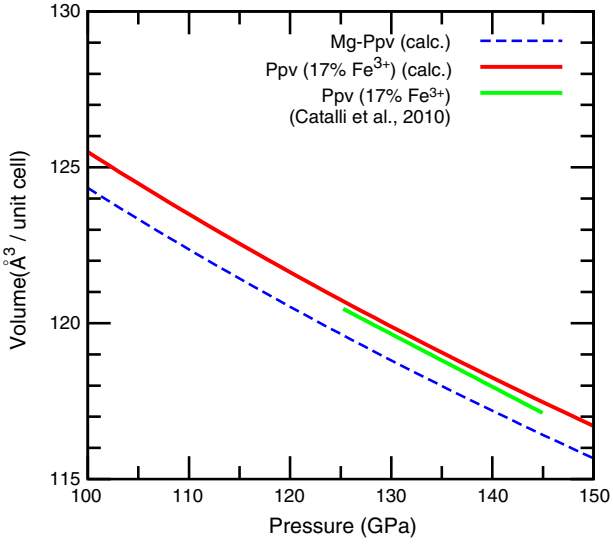

Fig. 7. Comparison between calculation (LDA + U_{sc}, red line) and experiment (green line, Catalli et al., 2010a) on the volume-pressure equation of state of Fe^{3+}-bearing Ppv (Fig. 1b). The iron content studied here is 17% which is defined as the sum of iron ratios at the A and B sites. Volume of the Mg-end member Ppv is shown as a reference (this calculation, dashed line). (For interpretation of the references to color in this figure legend, the reader is referred to the web version of this article.)

4. Conclusions

We have investigated the spin states and quadrupole splittings of iron incorporated in $MgSiO_3$ post-perovskite using DFT + U calculations. We found that Fe^{2+} remains in the HS state throughout the D″ pressure range. The computed QS of this state, 3.09–3.67 mm/s, is in good agreement with that extracted from Mössbauer spectra, 3.77 ± 0.25 mm/s. The IS and LS Fe^{2+} are energetically unfavorable, and their QSs are very different from those extracted from Mössbauer spectra. A pair of Fe^{3+} ions that substitute for the nearest-neighbor Mg^{2+} (A-site) and Si^{4+} (B-site) pair prefer HS at the A site and LS at the B site at the D″ pressure range. The calculated QSs for this state also agree well with experiments. The calculated equation of states shows that Fe^{2+} and Fe^{3+} are equally effective in expanding the unit cell volume, but neither has an appreciable effect on the bulk modulus.

Acknowledgments

This work is supported by the NSF grants EAR-0810272, EAR-1047629, and partially by the MRSEC Program of NSF grants DMR-0212302 and DMR-0819885. We thank Peter Blaha for valuable discussions on the calculations of EFG via the WIEN2k code. All calculations were performed at the Minnesota Supercomputing Institute (MSI).

References

Anisimov, V.I., Zaanen, J., Andersen, O.K., 1991. Band theory and Mott insulators: Hubbard *U* instead of Stoner *I*. Phys. Rev. B 44 (3), 943–954.
Badro, J., Fiquet, G., Guyot, F., Rueff, J., Struzhkin, V.V., Vankó, G., Monaco, G., 2003. Iron partitioning in earth's mantle: toward a deep lower mantle discontinuity. Science 300, 789–791.
Bengtson, A., Li, J., Morgan, D., 2009. Mössbauer modeling to interpret the spin state of iron in (Mg, Fe) SiO_3 perovskite. Geophys. Res. Lett. 36, L15301.
Blaha, P., Schwarz, K., Madsen, G.K.H., Kvasnicka, D., Luitz, J., 2001. In: Schwarz, K. (Ed.), WIEN2k, Augmented Plane Wave + Local Orbitals Program for Calculating Crystal Properties. Techn. Universität Wien, Vienna.
Campo, V.L., Cococcioni, M., 2010. Extended DFT + U + V method with on-site and inter-site electronic interactions. J. Phys. Condens. Matter 22 (5), 055602.
Caracas, R., 2010. Spin and structural transitions in $AlFeO_3$ and $FeAlO_3$ perovskite and post-perovskite. Phys. Earth Planet. Inter. 182, 10–17.
Caracas, R., Cohen, R.E., 2008. Ferrous iron in post-perovskite from first-principles calculations. Phys. Earth Planet. Inter. 168, 147–152.
Catalli, K., Shim, S.H., Prakapenka, V.B., Zhao, J., Sturhahn, W., 2010a. X-ray diffraction and Moessbauer spectroscopy of Fe^{3+}-bearing Mg-silicate post-perovskite at 128–138 GPa. Am. Mineral. 95, 418–421.
Catalli, K., Shim, S.-H., Prakapenka, V.B., Zhao, J., Sturhahn, W., Chow, P., Xiao, Y., Liu, H., Cynn, H., Evans, W.J., 2010b. Spin state of ferric iron in $MgSiO_3$ perovskite and its effect on elastic properties. Earth Planet. Sci. Lett. 289, 68–75.
Ceperley, D.M., Alder, B.J., 1980. Ground state of the electron gas by a stochastic method. Phys. Rev. Lett. 45, 566–569.
Cococcioni, M., de Gironcoli, S., 2005. Linear response approach to the calculation of the effective interaction parameters in the LDA + U method. Phys. Rev. B 71 (3), 035105.
Crowhurst, J.C., Brown, J.M., Goncharov, A.F., Jacobsen, S.D., 2008. Elasticity of (Mg, Fe) O through the spin transition of iron in the lower mantle. Science 319, 451–453.
Giannozzi, P., et al., 2009. QUANTUM ESPRESSO: a modular and open-source software project for quantum simulations of materials. J. Phys. Condens. Matter 21, 5502.
Goncharov, A.F., Struzhkin, V.V., Jacobsen, S.D., 2006. Reduced radiative conductivity of low-spin (Mg, Fe)O in the lower mantle. Science 312, 1205–1207.
Hsu, H., Blaha, P., Wentzcovitch, R.M., Leighton, C., 2010a. Cobalt spin states and hyperfine interactions in $LaCoO_3$ investigated by LDA + U calculations. Phys. Rev. B 82 (10), 100406.
Hsu, H., Wentzcovitch, R.M., Cococcoini, M., 2010b. Spin states and hyperfine interactions of iron in (Mg, Fe) SiO# perovskite under pressure. Earth Planet. Sci. Lett. 294 (1–2), 19–26.
Hsu, H., Blaha, P., Cococcioni, M., Wentzcovitch, R.M., 2011. Spin-state crossover and hyperfine interactions of ferric iron in $MgSiO_3$ perovskite. Phys. Rev. Lett. 106 (11), 118501.
Jackson, J.M., Sturhahn, W., Tschauner, O., Lerche, M., Fei, Y., 2009. Behavior of iron in (Mg, Fe) SiO_3 post-perovskite assemblages at Mbar pressures. Geophys. Res. Lett. 36, L10301.
Kohn, W., Sham, L.J., 1965. Self-consistent equations including exchange and correlation effects. Phys. Rev. 140, 1133–1138.
Kulik, H.J., Cococcioni, M., Scherlis, D.A., Marzari, N., 2006. Density functional theory in transition-metal chemistry: a self-consistent Hubbard *U* approach. Phys. Rev. Lett. 97 (10), 103001.

Lay, T., Garnero, E.J., 2007. Reconciling the post-perovskite phase with seismological observations of lowermost mantle structure. In: Hirose, K., Brodholt, J., Lay, T., Yuen, D. (Eds.), Post-perovskite: the last mantle phase transition. : Geophy. Monogr., 174. American Geophysical Union, pp. 129–154.

Lin, J., Watson, H., Vankó, G., Alp, E.E., Prakapenka, V.B., Dera, P., Struzhkin, V.V., Kubo, A., Zhao, J., McCammon, C., Evans, W.J., 2008. Intermediate-spin ferrous iron in lowermost mantle post-perovskite and perovskite. Nat. Geosci. 1, 688–691.

Madsen, G.K.H., Blaha, P., Schwarz, K., Sjöstedt, E., Nordström, L., 2001. Efficient linearization of the augmented plane-wave method. Phys. Rev. B 64, 195134.

Mao, Z., Lin, J.F., Jacobs, C., Watson, H.C., Xiao, Y., Chow, P., Alp, E.E., Prakapenka, V.B., 2010. Electronic spin and valence states of Fe in $CaIrO_3$-type silicate post-perovskite in the Earth's lowermost mantle. Geophys. Res. Lett. 37, L22304.

McCammon, C., Kantor, I., Narygina, O., Rouquette, J., Ponkratz, U., Sergueev, I., Mezouar, M., Prakapenka, V., Dubrovinsky, L., 2008. Stable intermediate-spin ferrous iron in lower-mantle perovskite. Nat. Geosci. 1, 684–687.

McCammon, C., Dubrovinsky, L., Narygina, O., Kantor, I., Wu, X., Glazyrin, K., Sergueev, I., Chumakov, A.I., 2010. Low-spin Fe^{2+} in silicate perovskite and a possible layer at the base of the lower mantle. Phys. Earth Planet. Inter. 180, 215–221.

Monkhorst, H.J., Pack, J.D., 1976. Special points for Brillouin-zone integrations. Phys. Rev. B 13, 5188–5192.

Murakami, M., Hirose, K., Kawamura, K., Sata, N., Ohishi, Y., 2004. Post-perovskite phase transition in $MgSiO_3$. Science 304, 855–858.

Núñez-Valdez, M., Umemoto, K., Wentzcovitch, R.M., 2010. Fundamentals of elasticity of $(Mg_{1-x}, Fe_x)_2SiO_4$ olivine. Geophys. Res. Lett. 37, L14308.

Oganov, A.R., Ono, S., 2004. Theoretical and experimental evidence for a post-perovskite phase of $MgSiO_3$ in Earth's D″ layer. Nature 430, 445–448.

Ono, S., Kikegawa, T., Ohishi, Y., 2006. Equation of state of $CaIrO_3$-type $MgSiO_3$ up to 144 GPa. Am. Mineral. 91 (2–3), 475–478.

Perdew, J.P., Zunger, A., 1981. Self-interaction correction to density-functional approximations for many-electron systems. Phys. Rev. B 23 (10), 5048–5079.

Perdew, J.P., Burke, K., Ernzerhof, M., 1996. Generalized gradient approximation made simple. Phys. Rev. Lett. 77, 3865–3868.

Petrilli, H.M., Blöchl, P.E., Blaha, P., Schwarz, K., 1998. Electric-field-gradient calculations using the projector augmented wave method. Phys. Rev. B 57 (23), 14690–14697 and references therein.

Shim, S.-H., Catalli, K., Hustoft, J., Kubo, A., Prakapenka, V.B., Caldwell, W.A., Kunz, M., 2008. Crystal structure and thermoelastic properties of $(Mg_{0.91}Fe_{0.09})$ SiO_3 post-perovskite up to 135 GPa and 2700 K. Proc. Natl. Acad. Sci. U. S. A. 105, 7382–7386.

Tsuchiya, T., Tsuchiya, J., Umemoto, K., Wentzcovitch, R.M., 2004. Phase transition in $MgSiO_3$ perovskite in the earth's lower mantle. Earth Planet. Sci. Lett. 224, 241–248.

Tsuchiya, T., Wentzcovitch, R.M., da Silva, C.R.S., de Gironcoli, S., 2006. Spin transition in magnesiowüstite in Earth's lower mantle. Phys. Rev. Lett. 96 (19), 198501.

Umemoto, K., Hsu, H., Wentzcovitch, R.M., 2010. Effect of site degeneracies on the spin crossovers in (Mg, Fe) SiO_3 perovskite. Phys. Earth Planet. Inter. 180 (3–4), 209–214.

Wentzcovitch, R.M., Martins, J.L., Price, G.D., 1993. Ab initio molecular dynamics with variable cell shape: application to $MgSiO_3$. Phys. Rev. Lett. 70, 3947–3950.

Wentzcovitch, R.M., Justo, J.F., Wu, Z., da Silva, C.R.S., Yuen, D.A., Kohlstedt, D., 2009. Anomalous compressibility of ferropericlase throughout the iron spin cross-over. Proc. Natl. Acad. Sci. U. S. A. 106 (21), 8447.

Wu, Z., Justo, J.F., da Silva, C.R.S., de Gironcoli, S., Wentzcovitch, R.M., 2009. Anomalous thermodynamic properties in ferropericlase throughout its spin crossover transition. Phys. Rev. B 80 (1), 014409.

Yu, Y.G., Wentzcovitch, R.M., 2006. Density functional study of vibrational and thermodynamic properties of ringwoodite. J. Geophys. Res. 111, B12202.

Zhang, F., Oganov, A.R., 2006. Valence state and spin transitions of iron in Earth's mantle silicates. Earth Planet. Sci. Lett. 249, 436–443.